Gray Matter Functional Connectivity Networks by Integrating White Matter Signals: From Method, Properties and Applications

Zeqiang LinLi[1,4*], Zhuoyan Cai[1], Kang Hu[2,4], Chuchu Zheng[3], Wei Zhao[4], Shuixi Guo[4*]

Author Affiliations:

[1] School of Mathematics and Statistics, Guangdong University of Foreign Studies, Guangzhou, P.R. China

[2] School of Information Engineering, Wuhan Business University, Wuhan, P.R. China

3 School of Public Health, Shanxi Medical University, Taiyuan, P.R. China

[4] MOE-LCSM, School of Mathematics and Statistics, Hunan Normal University, Changsha, P. R. China

Corresponding author:

Shuixia Guo, Ph.D., School of Mathematics and Statistics, Hunan Normal University, Changsha 410006, P.R. China. Email: guoshuixia75@163.com Phone: +86-13107019688

Zeqiang Linli, Ph.D., School of Mathematics and Statistics, Guangdong University of Foreign Studies, Guangzhou 510004, P.R. China. Email: linlizeqiang@163.com Phone: +86-16620164042

Abstract

Resting-state functional connectivity (FC) analysis has predominantly focused on gray matter (GM), overlooking the potential functional contributions of white matter (WM). However, emerging evidence suggests that WM BOLD signals may actively shape large-scale brain networks. In this study, we introduce a novel GM-WM-GM connectivity framework that explicitly integrates WM signals to enhance our understanding of functional communication pathways. Using six independent datasets, we establish the test-retest reliability, topological characteristics, and clinical relevance of the GM-WM-GM network. Our findings reveal that GM-WM-GM connectivity demonstrates robust short- and long-term reliability, comparable to traditional GM-GM networks, while capturing unique network features. Graph-theoretical analyses confirm that GM-WM-GM networks exhibit small-world properties, modularity, and distinct hub distributions, emphasizing WM's active role in functional architecture. Comparative analyses with GM-GM connectivity highlight increased sensitivity to inter-individual variability and functional coupling patterns mediated by WM pathways. Furthermore, we identify significant age-related connectivity changes, characterized by linear declines and nonlinear trajectories, with peak connectivity observed in early adulthood. In a clinical cohort, individuals with autism spectrum disorder (ASD) exhibit hyperconnectivity in GM-WM-GM networks, correlating with symptom severity, underscoring the model's diagnostic potential. Additionally, GM-WM-GM connectivity predicts cognitive performance, particularly in language and reasoning tasks, demonstrating its behavioral relevance. Collectively, these findings provide compelling evidence that WM-mediated FC contributes to functional brain organization and individual variability. The GM-WM-GM framework offers a more comprehensive perspective on neural communication, bridging the gap between structural and functional connectivity, and holds promise for advancing neuroimaging biomarkers in aging and neuropsychiatric disorders.

Keywords: Resting-State Functional Connectivity, Gray Matter-White Matter Connectivity, Brain Network, White Matter Functional Network

1. Introduction

Over the past two decades, resting-state functional magnetic resonance imaging (rs-fMRI) has been widely used to map synchronized activity across distributed brain regions—collectively termed functional connectivity (FC)[1,2]. This approach has substantially advanced our understanding of large-scale network organization, developmental and aging trajectories, and clinical alterations in neuropsychiatric disorders[3–5]. However, most rs-fMRI studies have traditionally focused on gray matter (GM), where neural activity is presumed to drive blood-oxygen-level-dependent (BOLD) signals. Consequently, white matter (WM) is often overlooked in connectivity frameworks—partly because of its lower BOLD amplitude and its longstanding classification as a primarily structural conduit between GM regions[6–8]. Nonetheless, mounting evidence challenges this assumption, suggesting that WM may participate more actively in functional network dynamics than previously recognized.

In line with this emerging perspective, a growing body of research indicates that WM BOLD signals may carry biologically meaningful information[9–12] and can influence large-scale connectivity[13–17]. By aligning with known fiber tracts and exhibiting significant correlations with GM, WM functional networks reveal that WM is neither silent nor passive[18]. Indeed, several studies have documented how altered WM–GM connectivity patterns emerge in aging[19] and various clinical conditions[20,21], underscoring the contribution of WM microstructure, electrophysiological synchronization, and genetic factors to functional network organization. These findings suggest that capturing WM activity may refine our understanding of long-range communication, potentially enhancing early detection of disease-related disruptions or subtle cognitive changes. In this context, an explicit GM-WM-GM approach may clarify how WM contributes to functional circuits, moving beyond the implicit assumption that WM simply facilitates GM–GM interactions.

Although most studies prioritize GM, recent work highlights that incorporating WM can significantly broaden our understanding of large-scale network organization[14,15]. Several groups have proposed GM-WM-GM frameworks, identifying WM as an additional node set rather than a mere anatomical conduit. For example, Gao et al. employed bipartite GM-WM networks to uncover age-

related functional changes[14], Zu et al. emphasized WM's "missing third dimension," [15] and Li et al. integrated functional and structural data to examine how WM shapes network topography[16]. Despite these advances, a consensus on constructing or interpreting GM-WM-GM connectivity remains elusive due to the difficulty of reliably capturing WM signals and linking them to specific GM regions. Nonetheless, acknowledging WM as an active partner can illuminate conduction delays, metabolic constraints, and other factors underlying long-range interactions. By explicitly modeling GM-WM-GM networks, researchers may detect functional couplings that escape purely GM-based analyses, offering a more comprehensive view of the brain's architecture and its links to cognition and behavior.

Despite increasing recognition of WM's functional relevance, it remains unclear how to systematically construct GM-WM-GM networks that explicitly incorporate WM signals. Here, we propose a novel method that quantifies how two GM regions connect via shared WM pathways, building on recent insights[14,15]. By treating WM as a dynamic bridge—rather than a passive relay—we aim to uncover subtle interactions that might remain hidden in standard GM-based analyses. Guided by this rationale, our study develops and validates an approach for constructing GM-WM-GM networks, assesses their test-retest reliability and topological organization, and compares them with conventional GM-GM connectivity. We further explore the practical value of GM-WM-GM networks by investigating age-related changes, clinical relevance, and associations with cognitive and behavioral measures. Through these integrated analyses, we seek to establish a comprehensive framework that illuminates the brain's functional architecture and bridges the gap between conventional GM-centric methods and WM's active role in inter-regional communication.

2. Results

2.1 General Description of Datasets, Analytical Methods, and Research Questions

In this study, we introduced a framework to construct GM-WM-GM FC networks by explicitly incorporating WM signals alongside conventional GM analyses. Briefly, after preprocessing each participant's rs-fMRI data, we extracted time-series signals from 90 GM regions (AAL atlas) and 48 WM bundles (JHU-ICBM 48 atlas), then computed a bipartite GM–WM correlation matrix. A final GM-WM-GM connectivity matrix was formed by quantifying how two GM regions are related via their shared variance in WM correlations.

To evaluate, characterize, and apply these GM-WM-GM networks from multiple perspectives—test-retest reliability, topological organization, comparisons to traditional GM-GM connectivity, age-related changes, clinical relevance, and cognitive/behavioral correlates—we drew on six independent datasets. The SLIM dataset was used for investigating long-term reliability and cross-session consistency, whereas BNU-3provided short-term reliability measurements. The SALD dataset offered a large cross-sectional sample to examine age trajectories of GM-WM-GM connectivity. Clinical relevance was explored using the ABIDE-II, focusing on disorder-specific alterations in WM-mediated networks. Finally, the BGSP dataset enabled partial least squares regression linking GM-WM-GM connectivity to various cognitive and behavioral measures. Table S1 (Supplementary Materials) summarizes the demographics and scanning protocols for each dataset. Unless specified otherwise, structural and functional MRI images in all datasets underwent a uniform preprocessing pipeline using SPM-based tools, after which we constructed GM-WM-GM networks following the approach outlined above. Figure 1 visually depicts the entire process.

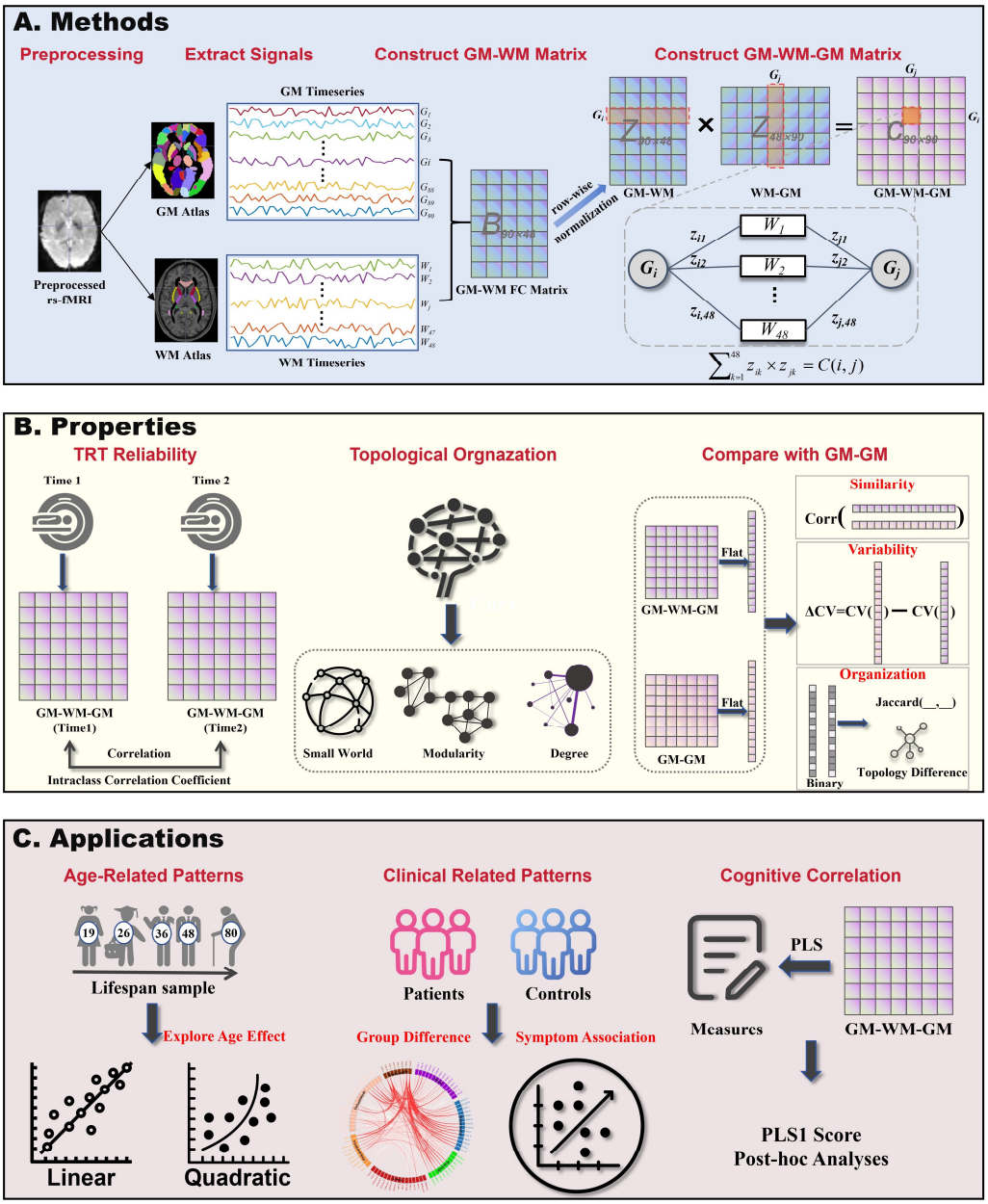

Figure 1. Schematic Representation of the Study Design. (A) Construction of the GM-WM-GM Network. This process began with extracting GM and WM signals from preprocessed rs-fMRI data to construct a GM-WM connectivity matrix B. Subsequently, the values were row-wise standardized to produce a Z-score matrix, emphasizing the relative interaction profile of each region within its connectivity pattern. Finally, the covariance matrix C, derived from Z, served as a GM FC matrix mediated by WM, also termed the GM-WM-GM FC network. (B) Characterization of GM-WM-GM Properties. The study examined the TRT reliability of the GM-WM-GM network and its topological properties through graph theoretical measures. Comparative analyses between GM-WM-GM and

traditional GM-GM connectivity networks were also conducted. (C) Applications of GM-WM-GM Networks. The practical utility of the GM-WM-GM network was explored in three domains. First, investigating its age-related patterns, including both linear and quadratic effects; second, assessing its application in clinical contexts; and third, employing partial least squares (PLS) regression to evaluate its predictive capacity for cognitive and behavioral measures.

2.2 GM-WM-GM Network Patterns

Following image preprocessing, all rs-fMRI data were segmented into 90 GM regions and 48 WM bundles. All GM nodes were categorized into six functional networks according to Yeo's functional parcellation of cerebral cortex (Figure 2A). We then computed a (90×48) bipartite GM-WM connectivity matrix and subsequently projected it into a (90×90) "GM-WM-GM" matrix by standardizing row-wise Z-scores and deriving their covariance (see Methods). At the group level, this GM-WM-GM matrix consistently displayed higher intra-network connectivity among large-scale functional subnetworks (e.g., default mode, sensorimotor) and moderately strong inter-network connections (Figure 2B). These baseline observations suggested that integrating WM signals could enrich our understanding of long-range communication.

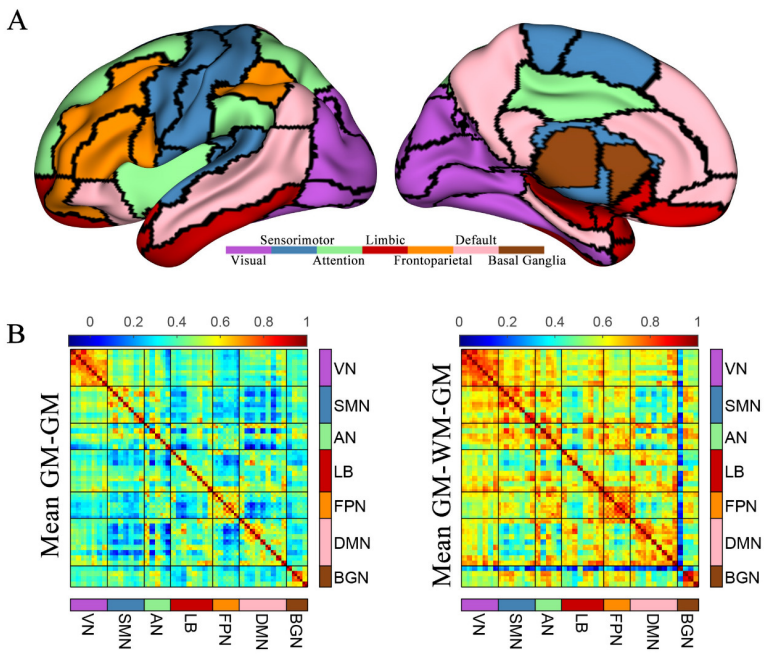

Figure 2. (A) A schematic representation of the division of 90 brain regions into seven large-scale

networks; **(B)** Group-level mean GM-GM connectivity strength matrix (r-value matrix) and GM-WM-GM connectivity strength matrix (normalized to a range of 0–1 for comparability).

2.3. Short- and Long-Term TRT Reliability

The BNU-3 dataset was used to estimate short-term TRT reliability, in which participants were scanned every three days over one month, whereas the SLIM dataset was used to estimate long-term TRT reliability, wherein participants were scanned three times (the average time intervals were 304.14, 515, and 817.87 days between the first and second scans, second and third scans, and first and third scans, respectively). As depicted in Figure 3A and 3B, the GM-WM-GM FC matrices exhibited consistent and stable patterns across different time points in both the SLIM and BNU-3 datasets at the group level. At the group-averaged level, GM-WM-GM connectivity networks demonstrated strong correlations across different time points, both in the long term ($r = 0.897$) and short term ($\text{mean}\, r = 0.955$). Additionally, we calculated the correlations between connectivity matrices at different time points at the individual subject level. In the SLIM dataset, the average Pearson correlation coefficient between two time points was 0.37 (±0.13), as shown in the lower-right corner of Figure 3A. Similarly, in the BNU-3 dataset, the average correlation coefficient across time points was approximately 0.53 ($r_{1,2} = 0.57; r_{1,3} = 0.52; r_{2,3} = 0.50$), as shown in the lower-right corner of Figure 3B.

We also quantified the TRT reliability of individual connections within the GM-WM-GM network using ICC measure. As shown in Figure 3C, the GM-WM-GM network exhibited a mean edge-wise ICC of 0.36 (±0.12) in the BNU-3 dataset, whereas the SLIM dataset demonstrated a mean edge-wise ICC of 0.20 (±0.08). These findings align with previous observations that long-term reliability is generally lower than short-term reliability, likely due to increased variability introduced by longer intervals between measurements (e.g., physiological changes and day-to-day fluctuations)[22,23].

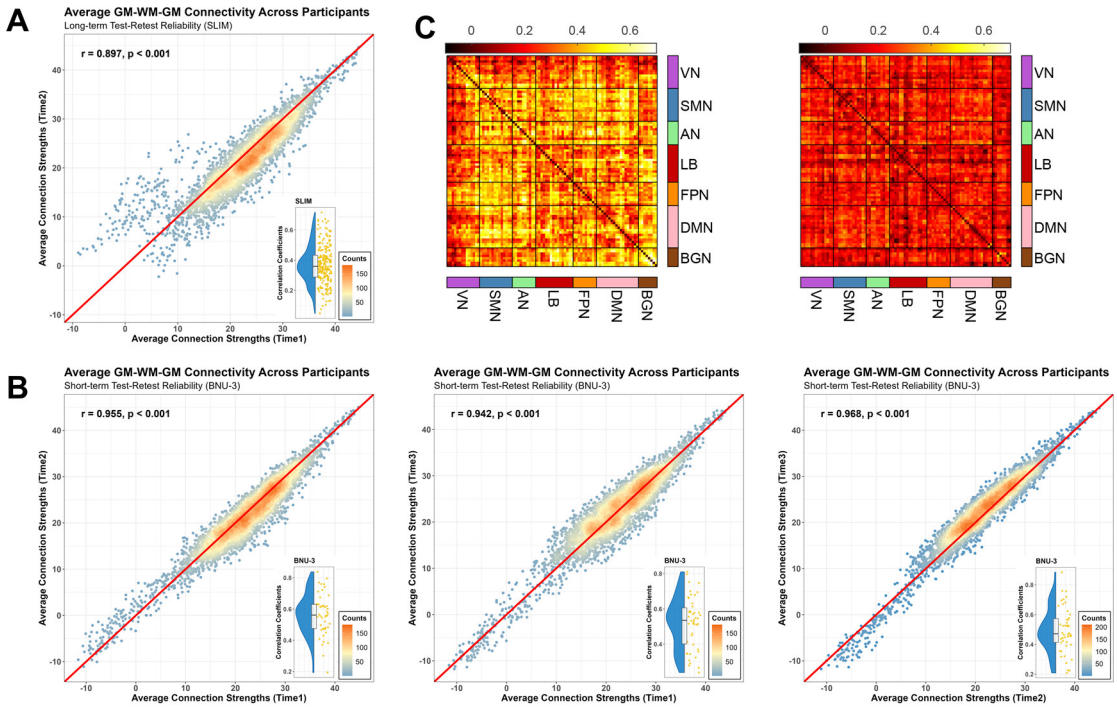

Figure 3. (A) Scatterplot of group-averaged GM-WM-GM connectivity strengths between two time points in the SLIM dataset. The X-axis represents connectivity strengths at time point 1, while the Y-axis represents those at time point 2. (B) Scatterplots of group-averaged GM-WM-GM connectivity strengths between each pair of three time points in the BNU-3 dataset. The X and Y axes correspond to connectivity strengths at the respective time points. (C) Heatmaps of edge-level ICC sparsity matrices, with the left panel depicting short-term test-retest reliability (TRT) and the right panel showing long-term ICC values. For (A) and (B), the inset in the lower-right corner of each plot illustrates raincloud plots of correlation coefficients at the subject level for GM-WM-GM connectivity networks across two time points.

2.4. Topological Organization of the GM-WM-GM Networks

2.4.1. Small-World Properties and Modularity

We used a sparsity-based thresholding procedure and computed various graph-theoretical measures via DPABINet[24]. Across multiple thresholds (0.10–0.34), GM-WM-GM networks consistently exhibited a small-world configuration, with normalized clustering coefficients >1 and characteristic path lengths near 1 (Figure 4A). Furthermore, the modularity coefficient (Q) remained above 0.3 across a wide threshold range (Figure 4B), suggesting that explicit WM inclusion produces well-segregated community

structures that may capture local clustering mechanisms more robustly than GM-only analyses.

2.4.2. Hub Distribution and Degree

The degree distribution of the group-level mean GM-WM-GM networks was best described by an exponentially truncated power-law model (Figure 4C), indicative of the presence of highly connected nodes, or hubs. These hubs are critical for maintaining efficient communication and integration within the network. Notably, 14 hub nodes were identified, distributed across the frontal, limbic, occipital, and temporal lobes (Figure 4D), emphasizing their pivotal roles in the brain's functional connectivity architecture.

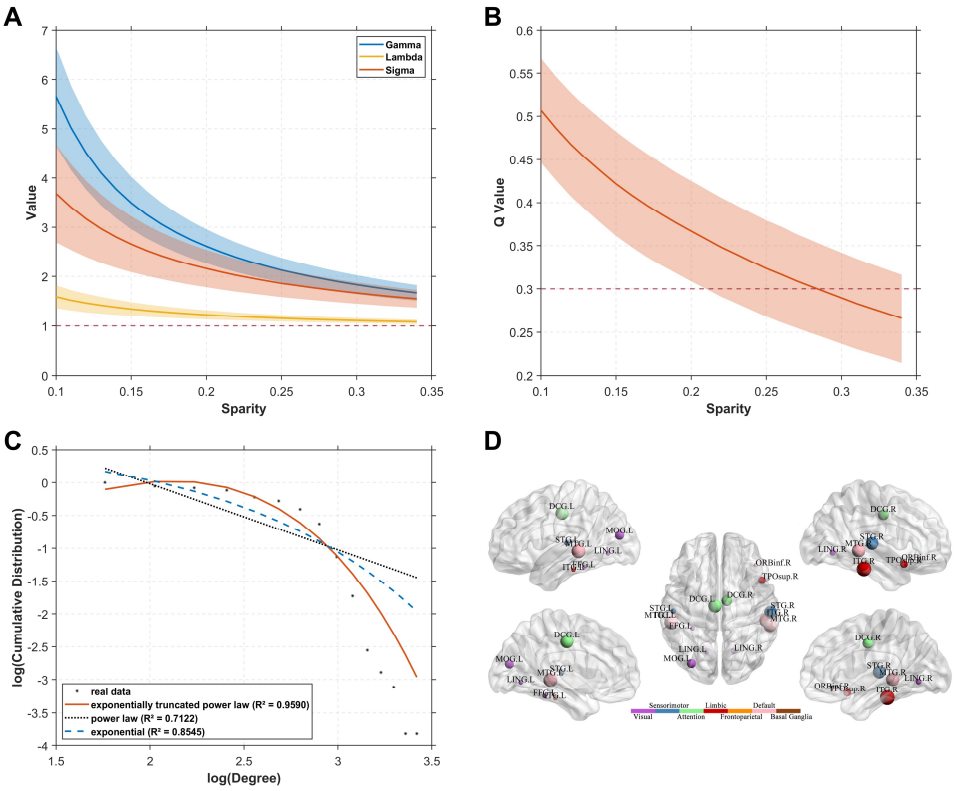

Figure 4. Topological Characterization of GM-WM-GM networks. (A) Small-world properties (σ), normalized clustering coefficient (γ), and normalized characteristic path length (λ) of the GM-WM-GM network across varying sparsity thresholds, presented as mean ± standard deviation. (B) Modularity coefficient (Q) of the GM-WM-GM network across different sparsity thresholds, also shown as mean ± standard deviation, demonstrating robust modularity. (C) Degree distribution of the group-averaged GM-WM-GM network, which is best described by an exponentially truncated power-law model, highlighting

the presence of highly connected brain regions. (D) Identification of 14 hub nodes within the group-averaged GM-WM-GM network, underscoring their critical roles in the brain's functional connectivity architecture.

2.5. Comparison with Traditional GM-GM Networks

2.5.1. Similarity Assessment

To assess the added value of WM-based modeling, we compared GM-WM-GM and GM-GM connectivity at the edge, network, and global levels. At the edge level, the GM-WM-GM and GM-GM FC networks exhibited a high degree of similarity, with an average Pearson correlation coefficient of 0.77 (±0.038). At the network level, the correlations between large-scale functional networks were stronger for inter-network connectivity ($\text{mean}\,r = 0.84$) than for intra-network connectivity ($\text{mean}\,r = 0.79$). At the global level, the GM-WM-GM and GM-GM FC networks demonstrated robust positive correlations across participants, with a global correlation coefficient of $r = 0.87$. These results indicate substantial consistency between the two methods, while also reflecting potential nuances in their respective functional connectivity profiles.

2.5.2. Variability Assessment

To further examine the differences between the two networks, we analyzed their variability using the CV as a metric of individual differences. At the edge level, we identified 480 edges with significant differences in CV values, of which 477 edges showed greater variability in the GM-WM-GM network, while the remaining 3 edges exhibited higher variability in the GM-GM network. At the network level, the GM-WM-GM network consistently displayed greater variability across all large-scale functional networks. At the global level, the GM-WM-GM network exhibited a significantly higher overall CV compared to the GM-GM network ($\triangle\text{CV} = 0.040, 99\%\text{CI}=[0.026,0.054]$). These findings highlight the GM-WM-GM network's increased sensitivity to individual variability, potentially due to its incorporation of white matter pathways.

2.5.3. Network Organization Assessment

Lastly, we explored the differences in network organization between the two methods. The Jaccard coefficients, which quantify structural similarity, revealed that the similarity between GM-WM-GM and GM-GM networks increased with higher sparsity thresholds (0.10 to 0.34). The average Jaccard coefficients ranged from 0.45 to 0.60, indicating reduced similarity at lower sparsity levels. These results suggest that sparsity thresholds substantially influence the apparent similarity between the two networks. Furthermore, the Jaccard coefficients varied across functional modules, reflecting differential organizational properties in specific subnetworks. This finding underscores the distinct contributions of white matter pathways to the functional network architecture captured by the GM-WM-GM approach.

To further compare the structural differences between GM-WM-GM and GM-GM FC networks, we analyzed a range of global and local graph-theoretical metrics. At the global level, the GM-GM network exhibited higher global efficiency and stronger small-worldness, indicating its capacity for efficient information integration and robust balance between segregation and integration. In contrast, the GM-WM-GM network demonstrated higher clustering coefficients and characteristic path lengths (λ), suggesting a more modular network organization. Additionally, the GM-WM-GM network exhibited higher assortativity, reflecting a tendency for highly connected nodes to preferentially connect with one another.

2.6. Age-Related Patterns in GM-WM-GM Networks

Using the SALD dataset, we examined how GM-WM-GM connectivity evolves with aging. Linear and quadratic models were fitted to connectivity strength, with age as the primary regressor and head motion/sex as covariates. Our analysis revealed significant age effects on more than half of the GM-WM-GM connections (2044/4005 edges, $P_{FDR} < 0.05$). These results highlight the extensive influence of age on the brain's white matter-mediated connectivity.

Specifically, as shown in Figure 6A, the majority of significant connections (1604 edges) exhibited negative linear relationships with age, while a smaller subset (40 edges) displayed positive linear relationships. These findings suggest that most GM-WM-GM connections weaken with advancing age, with a limited number strengthening over time. In addition to linear effects, quadratic age-related patterns

were observed in 400 connections (Figure 6B). Of these, 384 edges showed inverted U-shaped trajectories, indicating that connectivity strength peaks at a certain age before declining. Conversely, 16 edges demonstrated U-shaped trajectories, with connectivity decreasing initially and increasing later in life. The average peak age for connections with significant quadratic effects was calculated to be 33.84 years, suggesting a critical period of maximal connectivity in early adulthood.

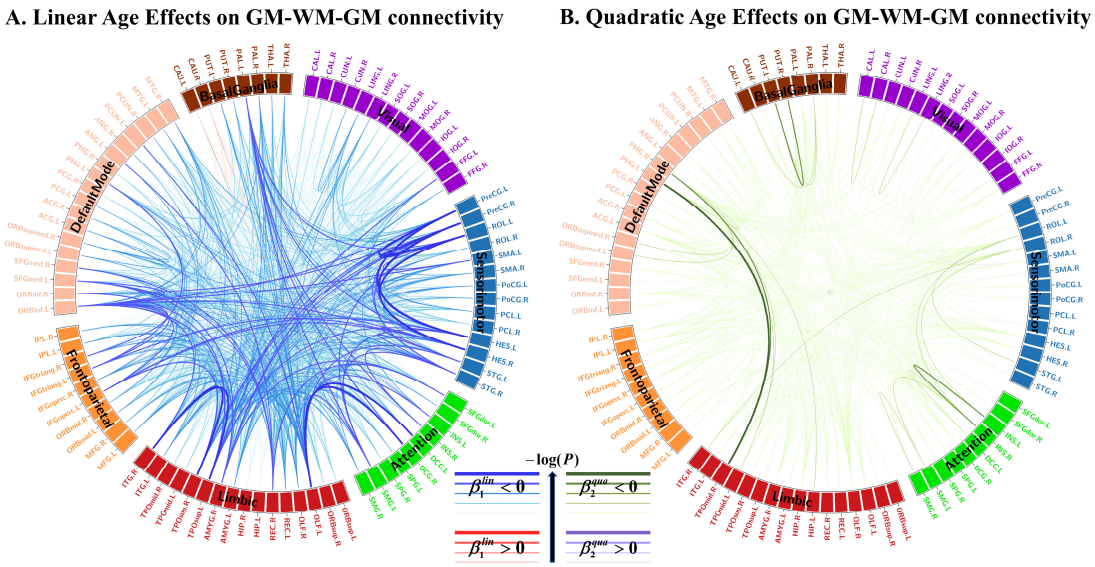

Figure 5. Age-Related Patterns of GM-WM-GM Networks. (A) Linear Effects of Age on GM-WM-GM Connectivity Networks. The thickness of the lines represents the magnitude of the effects, with blue lines indicating negative correlations and red lines indicating positive correlations. (B) Quadratic Effects of Age on GM-WM-GM Connectivity Networks. The thickness of the lines reflects the effect sizes, with green lines representing inverted U-shaped relationships and red lines denoting U-shaped relationships.

2.7. Clinical Relevance: Insights from Patient Cohorts

2.6.1. Neurological and Psychiatric Implications

To evaluate the clinical relevance of the GM-WM-GM FC network, we constructed GM-WM-GM connectivity networks for individuals with Autism Spectrum Disorder (ASD) and typically developing controls (TC) using the ABIDE-II dataset and conducted group comparisons. After controlling for covariates such as age, sex, and site effects, ASD exhibited significantly stronger global mean connectivity compared to TC ($t = 2.67, p = 0.0078$), as shown in **Figure 6A**. At the edge level, 526

GM-WM-GM connections were identified as significantly different between the two groups ($P_{FDR} < 0.05$), with all significant connections showing stronger connectivity in the ASD group (**Figure 6B**). Applying the same analysis to traditional GM-GM functional connectivity networks revealed only 41 significant edges, all of which also showed stronger connectivity in the ASD group. Importantly, as shown in **Figure 6C,** 88% (36/41) of these GM-GM connections overlapped with the GM-WM-GM connections identified, suggesting substantial convergence between the two approaches while highlighting the GM-WM-GM network's enhanced sensitivity in detecting group differences.

Next, we investigated whether the identified GM-WM-GM connections were associated with disease progression, as measured by the Autism Diagnostic Observation Schedule-Generic (ADOS-G). A total score and four sub-score were analyzed: total score (ADOS_G_TOTAL), communication (ADOS_G_COMM), social interaction (ADOS_G_SOCIAL), stereotyped behaviors (ADOS_G_STEREO_BEHAV), and creativity (ADOS_G_CREATIVITY). Our analysis revealed significant negative correlations between the mean GM-WM-GM connections and multiple ADOS-G measures, including the total score ($rho = -0.21, P_{FDR} = 0.0273$), ADOS_G_COMM ($rho = -0.19, P_{FDR} = 0.0273$), and ADOS_G_CREATIVITY ($rho = -0.31, P_{FDR} = 0.0342$), as shown in **Figure 6D**. At the edge level, 94 connections were significantly negatively correlated with ADOS_G_TOTAL, 61 with ADOS_G_COMM, 9 with ADOS_G_SOCIAL, and 59 with ADOS_G_CREATIVITY.

These findings indicate that stronger GM-WM-GM connectivity in ASD may reflect compensatory mechanisms or atypical neural communication pathways and underscore the potential of these connections as biomarkers for assessing disease severity and symptomatology.

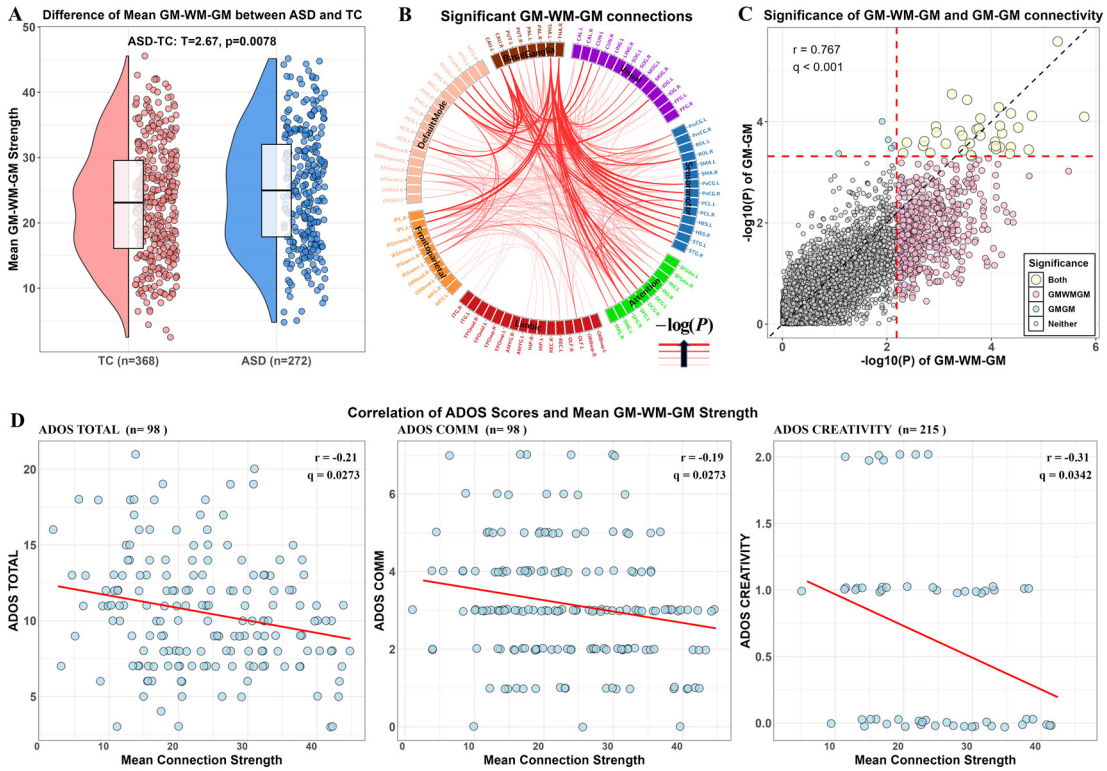

Figure 6. Comparative Analysis of GM-WM-GM Connectivity Between ASD and TC Groups. (A) Comparison of global-averaged GM-WM-GM connectivity strengths between ASD and TC groups. (B) Significantly different GM-WM-GM connections identified between ASD and TC groups, with all connections showing ASD > TC. Line thickness represents the magnitude of the effect. (C) Scatterplot comparing the p-values of group differences for GM-WM-GM and GM-GM function connections. The two red dashed lines indicate the maximum p-values passing FDR correction ($P_{FDR} < 0.05$). Data points are color-coded based on significance: light yellow for connections significant in both GM-WM-GM and GM-GM analyses, light red for connections significant only in GM-WM-GM, and light blue for connections significant only in GM-GM. (D) Correlation between the mean strength of significant GM-WM-GM differences and ADOS-G scores, including ADOS-G total, ADOS-G COMM and ADOS-G CREATIVITY. Spearman's correlation coefficient was used to quantify the strength of the association.

2.7. GM-WM-GM Correlations with Cognitive and Behavioral Measures

The BGSP dataset included a broad range of behavioral and cognitive measures, which allowed examining phenotypic correlates of GM-WM-GM FC networks. Specifically, we used the partial least-squares (PLS) regression to examine the ability of GM-WM-GM FC networks to explain interindividual

variance in 4 behavioral and cognitive phenotypes, including Shipley vocabulary score, matrix reasoning scores, Shipley and matrix reasoning estimated IQ. We found that the PLS1 scores derived from the GM-MW-GM explained significant proportions of interindividual variance in the Shipley vocabulary task ($8.95\%, P_{permutation} = 0.0229$) and estimated IQ derived from Shipley-Hartford Age-Corrected T-Scores ($9.09\%, P_{permutation} = 0.0186$) (**Figure 7**), whereas no significant results were found for the matrix reasoning score ($P_{permutation} = 0.728$) and estimated IQ derived through the OPIE3 formula ($P_{permutation} = 0.654$). For the prediction analyses, we found that the GM-MW-GM predicted individual scores of the Shipley vocabulary task ($\text{mean } r = 0.0813, P_{permutation} = 0.0255$), whereas no significant results were found for the estimated IQ derived from Shipley-Hartford Age-Corrected T-Scores ($\text{mean } r = 0.0505, P_{permutation} = 0.1088$).

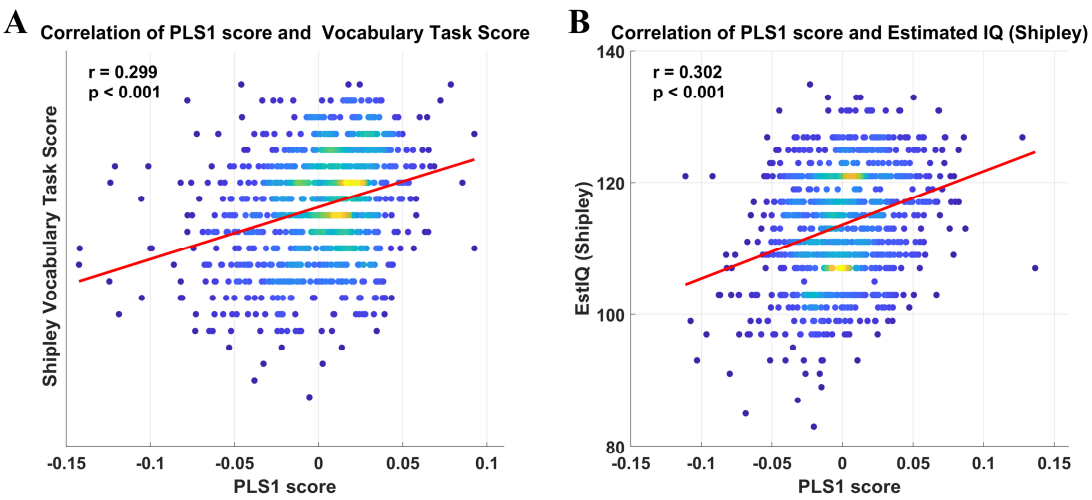

Figure 7. Association between GM-WM-GM connectivity and Behavior and Cognition measures. (A) Correlation between PLS1 scores and the Shipley vocabulary task scores; (B) Correlation between PLS1 scores and the estimated IQ derived from Shipley-Hartford Age-Corrected T-Scores.

3. Discussion

The present study set out to construct and validate a novel GM-WM-GM connectivity framework, with the aim of explicitly incorporating WM signals into functional analyses that have traditionally focused on GM alone. By examining test-retest reliability, network-level organization, and key differences compared to conventional GM-GM networks, our findings collectively highlight the

feasibility, reliability, and additional value of modeling WM as an active contributor to the brain's functional architecture. These results emphasize that, while GM remains the principal locus for metabolic and synaptic activity, WM is far from a passive conduit, potentially exerting meaningful influence on large-scale functional network configurations.

Our analyses underscore the first main finding: the GM-WM-GM network displayed robust test-retest reliability, with ICCs that are comparable to or even surpass those often reported for GM-GM connectivity. This observation suggests that the incorporation of WM signals not only preserves but may enhance the consistency of functional connectivity measures across scanning sessions and time intervals. Considering that measurement reliability forms the foundation of any methodological advancement, this outcome supports the idea that WM BOLD fluctuations, though typically lower in amplitude, can be harnessed in a stable and reproducible manner. It also aligns with emerging literature showing that systematic patterns in WM signals can be captured using state-of-the-art preprocessing and analysis methods[6].

Beyond reliability, our study provides evidence of a distinct topological profile in GM-WM-GM networks. Specifically, we observed differences in clustering coefficients, path lengths, and assortativity, when compared to GM-GM networks. These patterns highlight unique pathways by which WM might modulate or constrain neural communication. Recent work has similarly found that the inclusion of WM as functional nodes can alter modular structure and network integration, potentially reflecting microstructural or metabolic demands associated with conduction delays[14,15]. By treating WM as signal-bearing regions of the brain rather than mere structural cables, we may better capture the complexity of long-range connectivity that links distant GM regions. This expanded model may also help refine our understanding of how brain networks adapt or deteriorate in the context of aging and disease, where WM tracts can become compromised[16].

A third key insight emerged from comparing the GM-WM-GM approach to conventional GM-GM analyses at multiple scales, ranging from edge-level correlation patterns to global network properties. Although GM-WM-GM networks showed substantial overlap with GM-GM connections, we detected

edges exhibiting heightened variability in GM-WM-GM, as evidenced by significantly greater CV. Such findings raise the possibility that WM-inclusive models capture individual differences in a way that might be obscured by focusing solely on GM signals. Because WM microstructure varies markedly across individuals and is influenced by genetic and environmental factors[10,11], the variability uncovered in these edges could reflect biologically meaningful heterogeneity rather than mere methodological noise. Consequently, these novel GM-WM-GM connections may serve as powerful biomarkers for studying developmental trajectories, disease onset, or the effects of targeted interventions, if replicated in larger and more diverse samples.

Notably, our analyses also revealed meaningful age-related changes in GM-WM-GM networks. Older adults exhibited a reduction in WM-mediated connectivity in large-scale networks, such as the DMN and FPN, which are well known to undergo functional reorganization with age. These changes were often accompanied by decrements in cognitive performance, suggesting that the degradation of WM pathways may amplify the vulnerability of long-range interregional communication in aging[25]. By explicitly modeling WM, our framework captured subtle disruptions in network integration that might remain undetected using GM-based connectivity methods alone. This finding underscores the potential of GM-WM-GM connectivity as an early marker for cognitive decline and a valuable tool for distinguishing normal aging from pathological processes.

Several limitations should also be acknowledged. First, our primarily cross-sectional design precludes causal inferences or detailed longitudinal analyses. It remains possible, for instance, that WM disruption in clinical groups might precede or follow specific changes in GM connectivity over time. Second, though we addressed differences in signal amplitude and partial volume effects, the relatively subtle nature of WM BOLD signals calls for replication using larger, demographically varied cohorts. Third, we have not fully explored how dynamic fluctuations in WM and GM connectivity may interrelate moment-by-moment, a topic that could further elucidate how WM shapes transient coordination among cortical regions. Despite these caveats, our findings lay the groundwork for deeper, integrative investigations that blend structural, functional, and genetic data to clarify the fundamental role of white matter in the emerging field of multi-tissue connectomics.

4. Methods and Materials

4.1. Datasets

To comprehensively evaluate the constructed GM-WM-GM networks, we employed several independent datasets and conducted a systematic investigation from multiple perspectives. These analyses aimed to assess the networks' test-retest (TRT) reliability, elucidate their organizational principles, compare them with traditional GM-GM networks, and examine their associations with aging trajectories, clinical relevance, and behavioral and cognitive correlates.

Specifically, the Southwest University Longitudinal Imaging Multimodal (SLIM) dataset (http://dx.doi.org/10.15387/fcp_indi.retro.slim) was employed to investigate long-term TRT reliability and network topology, while the Beijing Normal University (BNU-3) dataset (http://dx.doi.org/10.15387/fcp_indi.corr.bnu3) was used to assess short-term TRT reliability. The Southwest University Adult Lifespan (SALD) dataset (https://fcon_1000.projects.nitrc.org/indi/retro/sald.html) and Chinese Human Connectome Project (CHCP) dataset (https://doi.org/10.11922/sciencedb.01374) were utilized to examine age-related trajectories in GM-WM-GM networks. The Autism Brain Imaging Data Exchange II (ABIDE-II) project (https://fcon_1000.projects.nitrc.org/indi/abide/abide_II.html) was analyzed to assess the clinical relevance of these networks. The Brain Genomics Superstruct Project (BGSP) was used to examine Behavioral and Cognitive Correlates of GM-WM-GM Networks. For a detailed description of these datasets, please refer to the Supplementary Materials (see "Study Datasets" section). **Table S1** provides a summary of the demographic details for each dataset.

4.2. Neuroimaging Preprocessing

Functional MRI images in all the datasets underwent the same analytical pipeline to construct GM-WM-GM networks unless stated otherwise.

All acquired images were subjected to preprocessing using a combination of the SPM12 toolbox (http://www.fil.ion.ucl.ac.uk/spm/software/spm12), DPARSF (http://rfmri.org/DPARSF) toolboxes. The preprocessing steps involved in this study were described extensively in the Supplementary Materials.

Briefly, the individual T1 images were segmented into WM, GM, and cerebrospinal fluid (CSF) using SPM12's New Segment algorithm and then normalized to the Montreal Neurological Institute (MNI) template. The rs-fMRI were removed the initial several time points, corrected for slice timing and head motion effects, and co-registered with the anatomical image. Subsequently, 24 motion-related parameters, the mean CSF signal and motion spikes were regressed out. The data were detrended and temporally filtered with a passband frequency of 0.01 - 0.10 Hz. Then, spatial smoothing was performed separately in the WM and GM using a kernel with 4 mm full-width half-maximum (FWHM). Finally, the processed images were normalized to the standard MNI template and resampled to 3 mm^3 voxels.

A manual quality control procedure was performed after preprocessing. The following criteria were used to assess data quality: (1) successful generation of all preprocessed results, (2) mean framewise displacement (FD) below 0.2 mm, and (3) visual inspection confirming satisfactory spatial normalization.

4.3. Construction of GM-WM-GM Functional Connectome

As depicted in **Figure 1**, using the widely recognized Anatomical Automatic Labeling (AAL) and JHU-ICBM 48 atlases, time series were extracted from 90 cortical GM regions (denoted as $g_i, i = 1, 2, ..., 90$) and 48 WM fiber bundles (denoted as $\mathrm{w}_j, j = 1, 2, ..., 48$), derived from preprocessed functional imaging data. A 90×48 GM-WM functional correlation matrix was computed, representing the interaction between GM regions and WM tracts. In graph-theoretical terms, this GM-WM correlation matrix forms a bipartite graph $\mathcal{G} = \{G, W, E, B\}$, consisting of two distinct sets of nodes ($g_i \in G, w_j \in W$) where edges only connect nodes from different groups (with *E* representing the set of edges and *B* representing the edge weights). The lack of within-group connections (i.e., no WM-WM or GM-GM links) results in the absence of closed triangular paths, which complicates the evaluation of important network properties such as global efficiency (Borgatti & Everett, 1997). To overcome this limitation, we propose a novel method that projects the original bipartite GM-WM network into a weighted unipartite network where only GM nodes are explicit, and WM nodes are implicit—referred to as the GM-WM-GM network.

Specifically, for each participant, the GM-WM correlation matrix (denoted as $B = (b_{ij})_{90\times48}$) is a 90

×48 matrix where each row represents the functional connectivity of a GM region with multiple WM regions. To account for variability in connectivity strength and ensure comparability across different GM regions, we applied row-wise Z-score normalization to ***B***, to normalize for overall connectivity strength differences across GM regions, yielding a normalized matrix ***Z***. This normalization is grounded in the biological principle that GM regions exhibit different levels of overall connectivity. By standardizing these values, the analysis emphasizes how each region interacts relative to its own connectivity profile, offering a clearer representation of the brain's functional organization. Next, we computed the covariance matrix ***C*** of ***Z'*** to represent the functional connectivity between GM regions mediated by WM pathways. Each element of the resulting 90×90 matrix $C = \left(c_{ij}\right)_{90\times 90} = Z \cdot Z'$ quantifies the communication strength between cortical region **i** and cortical region **j** via shared WM connections. Thus, ***C*** serves as a GM FC matrix mediated by WM, also known as the GM-WM-GM FC network. This approach highlights the relative FC between GM regions, allowing for the detection of subtle interactions while accounting for variations in connectivity magnitude. It facilitates deeper insights into network properties and the investigation of clinically relevant connectivity changes.

Additionally, all GM nodes were categorized into six functional networks according to Yeo's functional parcellation of cerebral cortex, including Visual Network (VN), Sensorimotor Network (SMN), Attention Network (AN), Limbic Network (LN), Frontoparietal Network (FPN), Default Mode Network (DMN), and Basal Ganglia Network (BGN), as shown in Figure 2A and Table S2. Detailed methods and the correspondence between regions and networks can be found in Supplementary Materials.

4.4. Test–Retest Reliability Analysis

To evaluate the reliability of GM-WM-GM FC, both long-term and short-term TRT reliability were assessed using the SLIM and BNU-3 datasets, respectively. First, we calculated the correlation between connectivity matrices at different time points at the individual subject level (e.g., the correlation between connectivity matrices at time 1 and time 2) and subsequently averaged these correlation coefficients at the group level. Furthermore, the Intraclass Correlation Coefficient (ICC) was used to quantify both short-term and long-term TRT reliability of GM-WM-GM networks. A two-way random-effects model for single-measure agreement, ICC(2, 1), was employed, accounting for both individual variability and

measurement consistency across time. Formally, for each edge in the GM-WM-GM FC networks, the ICC was calculated as:

$$ICC(2,1) = \frac{MS_b - MS_r}{MS_b + (k-1)MS_r + k(MS_e - MS_r)/n} \quad (1)$$

where MS_b is the mean square between subjects, MS_r is the mean square between measurements (time points), MSe is the mean square error, k is the number of scans per subject (2 for SLIM dataset and 3 for BNU-3), and n is the number of subjects. This formula enables the evaluation of GM-WM-GM functional connectivity reliability across time points.

4.5. Topological Analysis of GM-WM-GM Networks

Before analyzing the topological properties of the GM-WM-GM networks, a sparsity-based thresholding procedure was applied to convert the weighted networks into binary representations. Sparsity is defined as the ratio of actual edges to the maximum possible edges in the network. By applying subject-specific thresholds, this procedure ensures a consistent number of edges across participants and sessions under different analytical approaches. Given the absence of a definitive sparsity standard, we adopted a range of [0.10, 0.34] with an interval of 0.01, following the default settings in DPABINet[24]. This range ensures that the resulting binary networks remain both sparse and estimable for small-world analysis. Subsequently, various graph-based network measures, including small-world properties, modularity, and degree, were calculated using the DPABINet toolbox. Detailed formulas and interpretations of these measures are available in the relevant literature[26]. For this analysis, we utilized the SLIM time1 dataset.

Small world Organization

Firstly, to determine whether the GM-WM-GM network exhibits small-world properties, commonly observed in brain networks, we calculated key small-world metrics such as the clustering coefficient and characteristic path length for each subject's connectivity network. These global measures were normalized by comparing them to the mean values of 100 randomly rewired networks, generated while preserving the degree distribution of the original networks. A network is considered to exhibit small-world properties if it shows a normalized clustering coefficient (γ) greater than 1 and a normalized

characteristic path length (λ) close to 1, indicating local clustering and global efficiency comparable to random networks.

Modularity

We also calculated the modularity coefficient Q, which quantifies the degree to which a network can be divided into distinct modules or communities. The Q value is between 0~1 and the real network modularity function value is generally between 0.3~0.7. Higher values of Q indicate a more pronounced modular structure, suggesting that the network is composed of tightly connected clusters with relatively sparse connections between them.

Degree Distribution

To investigate the roles of individual nodes in GM-WM-GM networks, we calculated the nodal degree for each network across a range of sparsity thresholds. In the context of brain networks, degree distributions often follow power-law-like distributions, suggesting a scale-free organization. Therefore, after averaging the nodal degree across participants and sparsity levels, we applied different models (power law, exponential, and exponentially truncated power law) to fit the degree distribution of the GM-WM-GM networks. Regions with average nodal degrees in the top 15% were classified as hubs.

4.6. Comparison of GM-WM-GM and GM-GM Networks

The GM-GM network captures direct functional interactions between GM regions, whereas the GM-WM-GM network incorporates WM pathways, thereby representing a more complex and indirect connectivity structure. It is crucial to determine whether the GM-WM-GM network provides unique information that offers additional value beyond the GM-GM network. To this end, we conducted a series of analyses across multiple dimensions, including edge-level correlations, population variability, and network organization, highlighting their similarities and differences.

Edge-Level and Network-Level Correlations

We first evaluated the similarities between the two networks through correlation analyses at three levels: edge, network, and global. At the edge level, Pearson correlation coefficients were calculated for

each connection, comparing the connectivity values derived from GM-WM-GM and GM-GM FC networks. At the network level, we computed the average intra-network and inter-network connectivity strengths across seven functional subnetworks for both methods and analyzed their correlation. Finally, at the global level, the mean connectivity values across all edges were calculated for each participant, and the correlation coefficients across participants were determined to assess the overall consistency between the two approaches.

Variability Assessment Using Coefficient of Variation (CV)

To further compare the two networks, we analyzed their variability across the population by calculating the coefficient of variation (CV) for each edge. The CV quantifies the relative variability of connection strengths, providing insights into individual differences. This comparison helps reveal whether the GM-WM-GM network captures unique variability patterns that may reflect its incorporation of white matter pathways. We evaluated the statistical significance of CV differences between the two methods using a bootstrap approach with 10,000 resampling iterations. This step highlights whether the GM-WM-GM FC network captures greater or lesser variability compared to the GM-GM network, reflecting its sensitivity to population heterogeneity.

Network Organization Analysis

Lastly, we explored the differences in network organization between the two methods. The Jaccard index was employed to measure the structural similarity between GM-WM-GM and GM-GM FC networks for each participant across a range of sparsity thresholds (0.10–0.34, with a step size of 0.01). Additionally, we computed global and local graph-theoretical metrics, including multiple global and local indices, using the DPABINet toolbox. These metrics provided a detailed comparison of the topological features of the two networks, revealing unique organizational properties attributable to the inclusion of white matter pathways in the GM-WM-GM FC network.

4.7. Age-Related Patterns of GM-WM-GM Networks

To investigate age-related patterns and understand how the GM-WM-GM FC network evolves over time, we employed linear models to analyze the trajectory of the GM-WM-GM network throughout

adulthood using the SALD dataset. The models considered both linear (in Eq. (1)) and quadratic terms (in Eq. (2)) to capture potential non-linear relationships as shown in the following formula, including sex and head motion (measured by mean FD) as covariables,

$$y = \beta_0^{lin} + \beta_1^{lin} \times Age + \beta_2^{lin} \times Sex + \beta_3^{lin} \times meanFD + \varepsilon, \tag{2}$$

$$y = \beta_0^{qua} + \beta_1^{qua} \times Age + \beta_2^{qua} \times Age^2 + \beta_3^{qua} \times Sex + \beta_4^{qua} \times meanFD + \varepsilon, \tag{3}$$

in which dependent variable is GM-WM-GM connectivity strength. The model selection was based on the best description of the trajectory of these measures throughout adulthood, determined by the Akaike Information Criterion (AIC). The significance tests of or were conducted by t-tests. In the results section, we reported standardized coefficients of or for the best-fit model. Additionally, for models exhibiting a significant quadratic effect of age, the peak age was calculated using the formula for the axis of symmetry in a quadratic function:

$$Age_{peak} = -\frac{\beta_1^{qua}}{2\beta_2^{qua}}. \tag{4}$$

4.8. Clinical Correlates of GM-WM-GM Networks

To evaluate the clinical relevance of the GM-WM-GM FC network, we constructed GM-WM-GM connectivity networks for individuals with Autism Spectrum Disorder (ASD) and typically developing controls (TC) using the ABIDE-II dataset and conducted group comparisons. For each edge, a two-sample t-test was performed to compare the two groups while accounting for covariates such as age, sex and site information. Additionally, we investigated the correlations between significant edges and clinical symptoms.

4.9. Behavioral and Cognitive Correlates of GM-WM-GM Networks

The BGSP dataset included a broad range of behavioral and cognitive measures, which allowed examining phenotypic correlates of GM-WM-GM FC networks. Specifically, we used the partial least-squares (PLS) regression to examine the ability of GM-WM-GM FC networks to explain interindividual variance in 4 behavioral and cognitive phenotypes, including shipley vocabulary score, matrix reasoning

scores, shipley and matrix reasoning estimated IQ. In the PLS regression model, the response variable was behavioral and cognitive data for a certain domain and the predictor variables were all edges in GM-WM-GM networks. Only the first component of the PLS model (i.e., PLS1) was examined, which was the linear combination of GM-WM-GM connections that exhibited the strongest correlation with the behavioral and cognitive data. Significance levels of the correlations were estimated by randomly shuffling the behavioral and cognitive data among participants (10000 times). For measures that showed significant associations with GM-WM-GM networks, we further employed the Brain Bias Set (BBS) modeling method to evaluate the predictive capacity of GM-WM-GM networks for individual scores.

Authors Contribution

Zeqiang Linli and Shuixia Guo conceived and designed the overall study. Zeqiang Linli oversaw data collection and verified the analytical methods. Zeqiang Linli, Zhuoyan Cai and Kang Hu performed data preprocessing, constructed the GM-WM-GM networks, and carried out the statistical analyses. Zeqiang Linli, Zhuoyan Cai and Kang Hu contributed to the methodology design and drafted large parts of the manuscript. Zeqiang Linli provided critical revisions, shaped the discussion of results, and coordinated manuscript editing. All authors discussed the results, commented on the manuscript at all stages, and approved the final version for publication.

Conflict of Interest Statement

The authors declare that they have no conflict of interest.

Financial support

Zeqiang Linli is supported by the Humanities and Social Sciences Youth Foundation of Ministry of Education of China (24YJCZH164), Guangzhou Basic and Applied Basic Research Project (2024A04J2776), Guangdong Province General University Characteristic Innovation projects (2024KTSCX178), and MOE-LCSM.

Data and Code Availability

Publicly available datasets were analyzed in this study. The analysis code will be made public after the article is accepted.

Reference

1. Biswal, B., Zerrin Yetkin, F., Haughton, V. M. & Hyde, J. S. Functional connectivity in the motor cortex of resting human brain using echo-planar mri. *Magn. Reson. Med.* **34**, 537–541 (1995).
2. Fox, M. D. & Raichle, M. E. Spontaneous fluctuations in brain activity observed with functional magnetic resonance imaging. *Nat. Rev. Neurosci.* **8**, 700–711 (2007).
3. Canario, E., Chen, D. & Biswal, B. A review of resting-state fMRI and its use to examine psychiatric disorders. *Psychoradiology* **1**, 42–53 (2021).
4. Sala-Llonch, R., Bartrés-Faz, D. & Junqué, C. Reorganization of brain networks in aging: A review of functional connectivity studies. *Front Psychol* **6**, 663 (2015).
5. van den Heuvel, M. P. & Hulshoff Pol, H. E. Exploring the brain network: a review on resting-state fMRI functional connectivity. *Eur. neuropsychopharmacol. : j. Eur. Coll. Neuropsychopharmacol.* **20**, 519–34 (2010).
6. Gawryluk, J. R., Mazerolle, E. L. & D'Arcy, R. C. N. Does functional MRI detect activation in white matter? A review of emerging evidence, issues, and future directions. *Front. Neurosci.* **8**, 239 (2014).
7. Grajauskas, L. A., Frizzell, T., Song, X. & D'Arcy, R. C. N. White matter fMRI activation cannot Be treated as a nuisance regressor: overcoming a historical blind spot. *Front. Neurosci.* **13**, 1024 (2019).
8. Chen, G. *et al.* BOLD response is more than just magnitude: improving detection sensitivity through capturing hemodynamic profiles. *Neuroimage* **277**, 120224 (2023).
9. Huang, Y. *et al.* Intracranial electrophysiological and structural basis of BOLD functional connectivity in human brain white matter. *Nat. Commun.* **14**, 3414 (2023).

10. Li, J. *et al.* Transcriptomic and macroscopic architectures of intersubject functional variability in human brain white-matter. *Commun. Biol.* **4**, 1417 (2021).

11. Ji, G.-J. *et al.* White matter dysfunction in psychiatric disorders is associated with neurotransmitter and genetic profiles. *Nat. Ment. Health* **1**, 655–666 (2023).

12. Ding, Z. *et al.* Detection of synchronous brain activity in white matter tracts at rest and under functional loading. *PNAS* **115**, 595–600 (2018).

13. Li, M. *et al.* Functional engagement of white matter in resting-state brain networks. *Neuroimage* **220**, 117096 (2020).

14. Gao, Y. *et al.* Functional alterations in bipartite network of white and grey matters during aging. *Neuroimage* **278**, 120277 (2023).

15. Zu, Z. *et al.* The missing third dimension-functional correlations of BOLD signals incorporating white matter. *Sci. Adv.* **10**, 616 (2024).

16. Li, M. *et al.* White matter engagement in brain networks assessed by integration of functional and structural connectivity. *Neuroimage* **302**, 120887 (2024).

17. Wang, L. *et al.* fMRI signals in white matter rewire gray matter community organization. *Neuroimage* **297**, 120763 (2024).

18. Peer, M., Nitzan, M., Bick, A. S., Levin, N. & Arzy, S. Evidence for Functional Networks within the Human Brain's White Matter. *J Neurosci* **37**, 6394–6407 (2017).

19. LinLi, Z., Hu, K., Guo, Q. & Guo, S. Static and dynamic connectivity structure of white-matter functional networks across the adult lifespan. *Prog. Neuro-Psychopharmacol. Biol. Psychiatry* **136**, 111252 (2025).

20. Chen, K. *et al.* Alteration of the large-scale white-matter functional networks in autism spectrum

disorder. *Cereb. cortex (N. Y. N.Y. : 1991)* **33**, 11582–11593 (2023).

21. Zhang, Y. *et al.* Desynchronized functional activities between brain white and gray matter in major depression disorder. *J. magn. reson. imaging : JMRI* **53**, 1375–1386 (2021).

22. Noble, S., Scheinost, D. & Constable, R. T. A decade of test-retest reliability of functional connectivity: A systematic review and meta-analysis. *Neuroimage* **203**, 116157 (2019).

23. Pannunzi, M. *et al.* Resting-state fMRI correlations: from link-wise unreliability to whole brain stability. *Neuroimage* **157**, 250–262 (2017).

24. Yan, C.-G., Wang, X.-D., Lu, B., Deng, Z.-Y. & Gao, Q.-L. DPABINet: a toolbox for brain network and graph theoretical analyses. *Sci. Bull.* **69**, 1628–1631 (2024).

25. Bennett, I. J. & Madden, D. J. Disconnected aging: cerebral white matter integrity and age-related differences in cognition. *Neuroscience* **276**, 187–205 (2014).

26. Rubinov, M. & Sporns, O. Complex network measures of brain connectivity: uses and interpretations. *Neuroimage* **52**, 1059–69 (2010).